Supplemental material

Validation of the aerosol transport model

Remote-sensing and in situ aerosol observations are not available over many Arctic Ocean areas due to harsh sampling conditions, extensive cloud cover, high sea ice albedo, and the long periods of darkness during polar night. To understand as best we can how aerosol microphysics impacts clouds over the Arctic, we used the FLEXPART dispersion model with black carbon as a proxy for combustion aerosols to identify clean (i.e., non-combustion aerosol dominated) conditions in Arctic air masses, so that cloud properties in these conditions could be compared to general observations.

From the limited black carbon (BC) data that are available, the FLEXPART model appears to capture BC aerosol patterns very well over the Arctic (Eckhardt et al., 2015; Stohl et al., 2015; Zamora et al., 2017). Unfortunately, a lack of observations makes it difficult to validate model BC concentrations and spatial distributions over large swaths of the Arctic, particularly in the free troposphere and during polar night. Because spatial biases in the FLEXPART output could influence the meaningfulness of statistical comparisons between different locations, we validated FLEXPART BC output with Cloud-Aerosol Lidar and Infrared Pathfinder Satellite Observation (CALIPSO) aerosol layer data, which are the only nighttime aerosol data available regionally over the Arctic.

Vertical aerosol layer distribution was obtained from CALIPSO v. 4.10 level 2, 5-km merged aerosol and cloud layer data (CALIPSO Science Team, 2016) at 532 nm. These data are collected at 30-m vertical resolution up to 8.2 km, and at 75-m resolution between 8.2-8.5 km. Aerosol-containing profiles were required to be cloud-free and to have cloud-aerosol detection (CAD) scores > 70, indicating high confidence in cloud and aerosol separation. For each clear-sky polar night profile during our sample period, we noted the fraction of each FLEXPART model vertical layer (0.6 to 1.5 km, 1.5 to 2.5 km, 2.5 to 4 km, 4 to 6 km, and 6 to 8.5 km) that was filled by an observed CALIPSO aerosol layer. From these fractions, ranging from 0 to 1, weighted averages were calculated on a horizontal basis at each altitude level over the Arctic Ocean region (see Figure S6).

CALIPSO aerosol profiles were used here for aerosol transport model validation. FLEXPART-derived clean conditions were more frequent at higher altitudes (Fig. 3), in line with previous observations of CALIPSO aerosol distributions (Di Pierro et al., 2013). Major uncertainties arise in this comparison because of the coarse vertical resolution of the FLEXPART model output, and because CALIPSO aerosols are not necessarily equivalent to BC concentrations. As such, it is unclear how observed CALIPSO aerosol layer thickness (measured in meters) would relate to the average BC concentration in an altitude range equivalent to the FLEXPART model's vertical resolution (measured in kilometers). For these reasons, and because we use the aerosol model in this study only to identify clean (BC < 30 ng m^{-3}) air masses, our validation efforts are focused mainly on assessing the likely locations of FLEXPART false negatives (i.e., where observations indicate that aerosol layers have a large impact on model-identified "clean" air masses). Some information on false positives is provided as well.

To estimate an upper limit of model BC false negatives from CALIPSO aerosol distributions, we make several assumptions. First, we assume that combustion aerosols are the dominant aerosol source over the Arctic during polar night at the altitudes of relevance during this study (0.6-8.5 km). Ground-based data and aerosol transport models indicate that this is a fairly reasonable assumption (Quinn et al., 2002, 2008; Stohl et al., 2002). Marine aerosols are mainly located in the shallow Arctic boundary layer. Mineral dust can be found throughout the Arctic atmosphere. However, although there are some local "sharp" dust plumes at some locations in the fall, wintertime local dust emissions are limited by extensive snow cover, and long-range transport of low-latitude dust is well mixed in the winter and, at moderate concentrations, is nearly omni-present in the Arctic free troposphere (Groot Zwaaftink et al., 2016).

We also assume that the BC contribution to combustion aerosol mass is steady, even though other studies have shown that OC:BC ratios, for example, can vary (Samset et al., 2018). In cases where the OC:BC ratio is higher than on average, FLEXPART would indicate relatively too little aerosol compared to cases with a low OC:BC ratio. Other uncertainties are introduced because CALIPSO cannot always identify dilute aerosol plumes (Kacenelenbogen et al., 2014), and it sometimes misclassifies ice clouds with very small ice particles as aerosol layers (Di Pierro, 2013). Despite these uncertainties, information from this analysis is still very useful because of how poorly the models are validated over large parts of the Arctic, particularly because these models provide the only regional estimates of combustion aerosol concentrations over large swaths of the Arctic.

Based on the above assumptions, model false negative rates in clean conditions are likely to be highest when CALIPSO aerosol layers are observed in a large fraction of the model altitude layer. Average "clean" FLEXPART vertical layers often contain some CALIPSO-observed aerosol layers within them. Based on a weighted-average grid analysis of data throughout the study period (Fig. S6a), CALIPSO aerosol layers are present in, on average, ~19-27% of FLEXPART layer volumes. The actual BC concentrations of these aerosol layers are unclear. Previous analysis indicates that CALIPSO misses ~33-36% of very dilute (30-50 ng BC m^{-3}) combustion aerosol layers (Zamora et al., 2017), and so the model false negative fractions estimated in Figure S6a might actually underestimate aerosol layer presence somewhat.

CALIPSO aerosol volume contributions in clean conditions were significantly less at each altitude level than those found in all or polluted (BC >150 ng m^{-3}) conditions (Wilcoxon rank test, $p < 0.05$) (Fig. S7). Most altitudes also had no major clustering of high values in Figure S6a, which provides some confidence that model-identified clean conditions are at least comparable between large regions (e.g., over sea ice and over open ocean). The largest clustering in Figure S6a occurs at the lowest altitude level (0.6-1.5 km), where there was a slightly higher likelihood of false negatives over open ocean compared to sea ice (pink line). The highest overall likelihood of false negatives occurred at the highest altitude level (6-8.5 km), but it was not much larger than at other altitudes (Fig. S7).

Previous analysis indicates that in nighttime clear-sky conditions, CALIPSO should detect (non-dilute) aerosol layers in profiles where FLEXPART reports median column BC concentrations greater than 150 ng m^{-3} (Zamora et al., 2017). Model false positive rates are be highest when CALIPSO aerosol layers do not fill a large fraction of the model altitude layer where modeled BC was >150 ng m^{-3} (Fig. S6b). CALIPSO detected aerosol layers nearly all the time during clear nighttime conditions in some portion of the altitude bin where high BC concentrations were predicted. These aerosol layers contributed to 0.3-2.0 times more volume on average, depending on altitude, than in clean conditions (Fig. S7). The likelihood of false positives was highest over the open ocean in the lower two altitude bins (0.6-2.5 km), which might have a small impact on our comparisons between sea ice and open ocean at these altitudes. Note that observed aerosol layers may be present in the model, but could be displaced in altitude (e.g., by a kilometer or two), which could contribute to the apparent false positives or false negatives.

In summary, for FLEXPART to correctly identify clean (i.e., low combustion aerosol) conditions, it needs to be able to correctly simulate the horizontal and vertical distributions of combustion aerosols. As mentioned in the main text, previously conducted model validation studies indicate that FLEXPART has skill in simulating the locations of BC transport over the Arctic. Here, we show that the volume of CALIPSO vertical aerosol layers is significantly smaller in model-estimated clean conditions in the vertical column than in all conditions, or in model-identified polluted conditions. This result indicates that FLEXPART also has some skill in the vertical layer prediction of BC aerosols over the Arctic Ocean. Moreover, we observed no major spatial biases in the false negative rates that would preclude the regional comparisons between sea ice and open ocean regions. Together, these findings and previous work support the use of FLEXPART for identifying clean conditions for the purposes of this study.

References

CALIPSO Science Team: CALIPSO/CALIOP Level 2, Lidar 5km Merged Aerosol and Cloud Layer Data, version 4.10, Hampton, VA, USA: NASA Atmospheric Science Data Center (ASDC), Accessed Nov. 2, 2017 at doi: 10.5067/CALIOP/CALIPSO/LID_L2_05kmMLay-Standard-V4-10, 2016.

Di Pierro, M.: Spatial and temporal distribution of Arctic aerosols: new insights from the CALIPSO satellite, Dissertation, University of Washington., 2013.

Di Pierro, M., Jaeglé, L., Eloranta, E. W. and Sharma, S.: Spatial and seasonal distribution of Arctic aerosols observed by the CALIOP satellite instrument (2006–2012), Atmos Chem Phys, 13(14), 7075–7095, doi:10.5194/acp-13-7075-2013, 2013.

Eckhardt, S., Quennehen, B., Olivié, D. J. L., Berntsen, T. K., Cherian, R., Christensen, J. H., Collins, W., Crepinsek, S., Daskalakis, N., Flanner, M., Herber, A., Heyes, C., Hodnebrog, Ø., Huang, L., Kanakidou, M., Klimont, Z., Langner, J., Law, K. S., Lund, M. T., Mahmood, R., Massling, A., Myriokefalitakis, S., Nielsen, I. E., Nøjgaard, J. K., Quaas, J., Quinn, P. K., Raut, J.-C., Rumbold, S. T., Schulz, M., Sharma, S., Skeie, R. B., Skov, H., Uttal, T., von Salzen, K. and Stohl, A.: Current model capabilities for simulating black carbon and sulfate concentrations in the Arctic atmosphere: a multi-model evaluation using a comprehensive measurement data set, Atmos Chem Phys, 15(16), 9413–9433, doi:10.5194/acp-15-9413-2015, 2015.

Groot Zwaaftink, C. D., Grythe, H., Skov, H. and Stohl, A.: Substantial contribution of northern high-latitude sources to mineral dust in the Arctic, J. Geophys. Res. Atmospheres, 121(22), 13,678-13,697, doi:10.1002/2016JD025482, 2016.

Kacenelenbogen, M., Redemann, J., Vaughan, M. A., Omar, A. H., Russell, P. B., Burton, S., Rogers, R. R., Ferrare, R. A. and Hostetler, C. A.: An evaluation of CALIOP/CALIPSO's aerosol-above-cloud detection and retrieval capability over North America, J. Geophys. Res. Atmospheres, 119(1), 230–244, doi:10.1002/2013JD020178, 2014.

Quinn, P. K., Miller, T. L., Bates, T. S., Ogren, J. A., Andrews, E. and Shaw, G. E.: A 3-year record of simultaneously measured aerosol chemical and optical properties at Barrow, Alaska, J. Geophys. Res., 107(D11), 4130, doi:10.1029/2001JD001248, 2002.

Quinn, P. K., Bates, T. S., Baum, E., Doubleday, N., Fiore, A. M., Flanner, M., Fridlind, A., Garrett, T. J., Koch, D., Menon, S., Shindell, D., Stohl, A. and Warren, S. G.: Short-lived pollutants in the Arctic: their climate impact and possible mitigation strategies, Atmos Chem Phys, 8(6), 1723–1735, doi:10.5194/acp-8-1723-2008, 2008.

Samset, B. H., Stjern, C. W., Andrews, E., Kahn, R. A., Myhre, G., Schulz, M. and Schuster, G. L.: Aerosol Absorption: Progress Towards Global and Regional Constraints, Curr. Clim. Change Rep., 1–19, doi:10.1007/s40641-018-0091-4, 2018.

Stohl, A., Eckhardt, S., Forster, C., James, P. and Spichtinger, N.: On the pathways and timescales of intercontinental air pollution transport, J. Geophys. Res. Atmospheres, 107(D23), 4684, doi:10.1029/2001JD001396, 2002.

Stohl, A., Aamaas, B., Amann, M., Baker, L. H., Bellouin, N., Berntsen, T. K., Boucher, O., Cherian, R., Collins, W., Daskalakis, N., Dusinska, M., Eckhardt, S., Fuglestvedt, J. S., Harju, M., Heyes, C., Hodnebrog, Ø., Hao, J., Im, U., Kanakidou, M., Klimont, Z., Kupiainen, K., Law, K. S., Lund, M. T., Maas, R., MacIntosh, C. R., Myhre, G., Myriokefalitakis, S., Olivié, D., Quaas, J., Quennehen, B., Raut, J.-C., Rumbold, S. T., Samset, B. H., Schulz, M., Seland, Ø., Shine, K. P., Skeie, R. B., Wang, S., Yttri, K. E. and Zhu, T.: Evaluating the climate and air quality impacts of short-lived pollutants, Atmos Chem Phys, 15(18), 10529–10566, doi:10.5194/acp-15-10529-2015, 2015.

Zamora, L. M., Kahn, R. A., Eckhardt, S., McComiskey, A., Sawamura, P., Moore, R. and Stohl, A.: Aerosol indirect effects on the nighttime Arctic Ocean surface from thin, predominantly liquid clouds, Atmos Chem Phys, 17(12), 7311–7332, doi:10.5194/acp-17-7311-2017, 2017.

Supplementary Figures

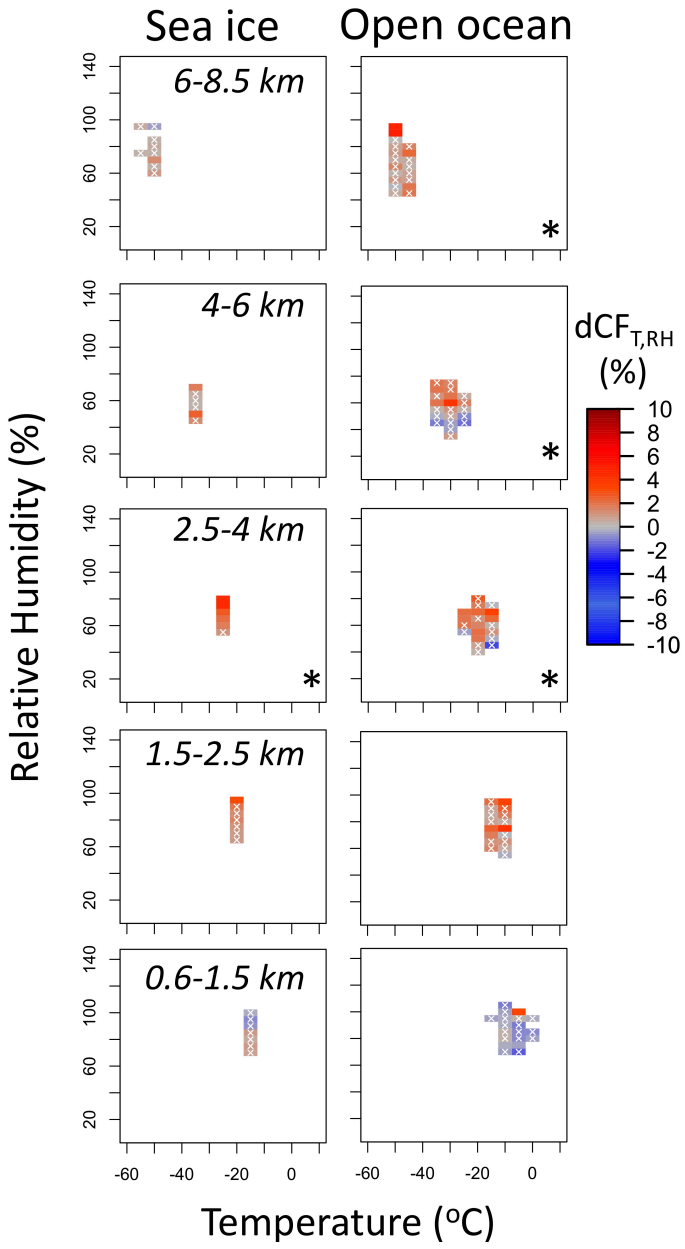

Figure S1. Same as for Figure 1, except for plotted only for Fall (September-November), with panels where individually significant cells numbered more than expected at random (binomial test, $p < 0.001$) marked with an asterisk (*). The shorter time frame results in fewer plotted cells compared to Figure 1, as plotted grid cells are required to each contain ≥ 7500 km^2 of gridded observations for illustration purposes.

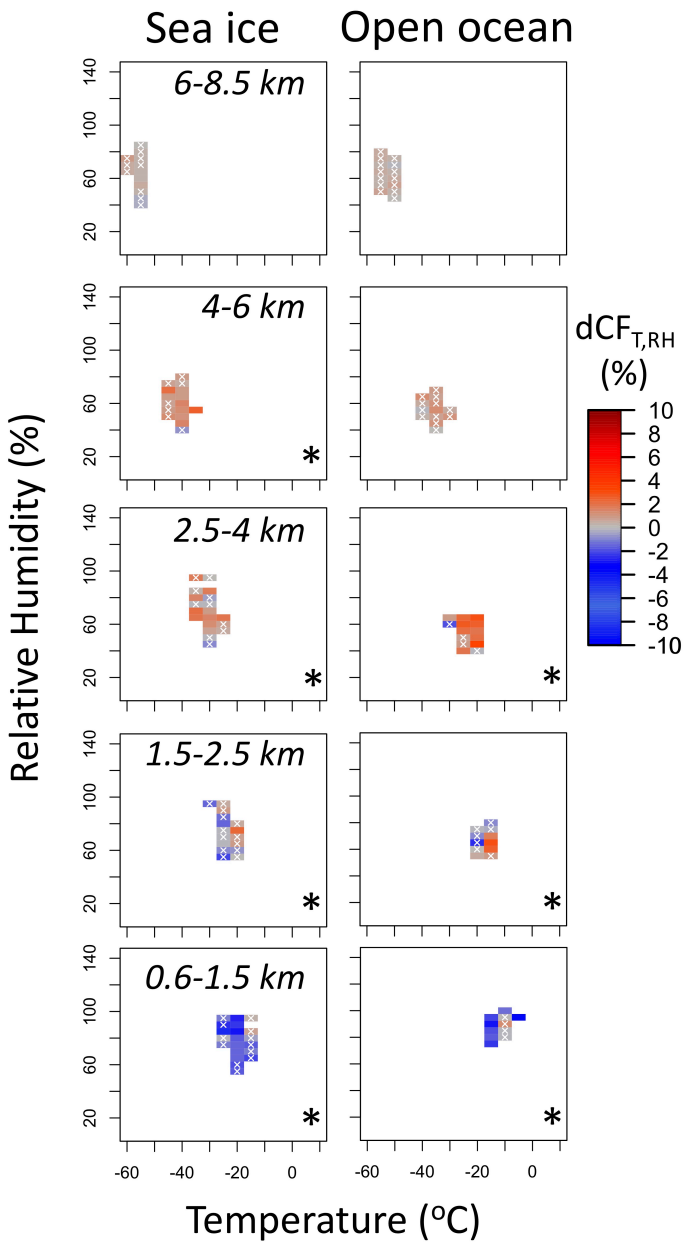

Figure S2. Same as for Figure S1, except for plotted only for Winter (December-February).

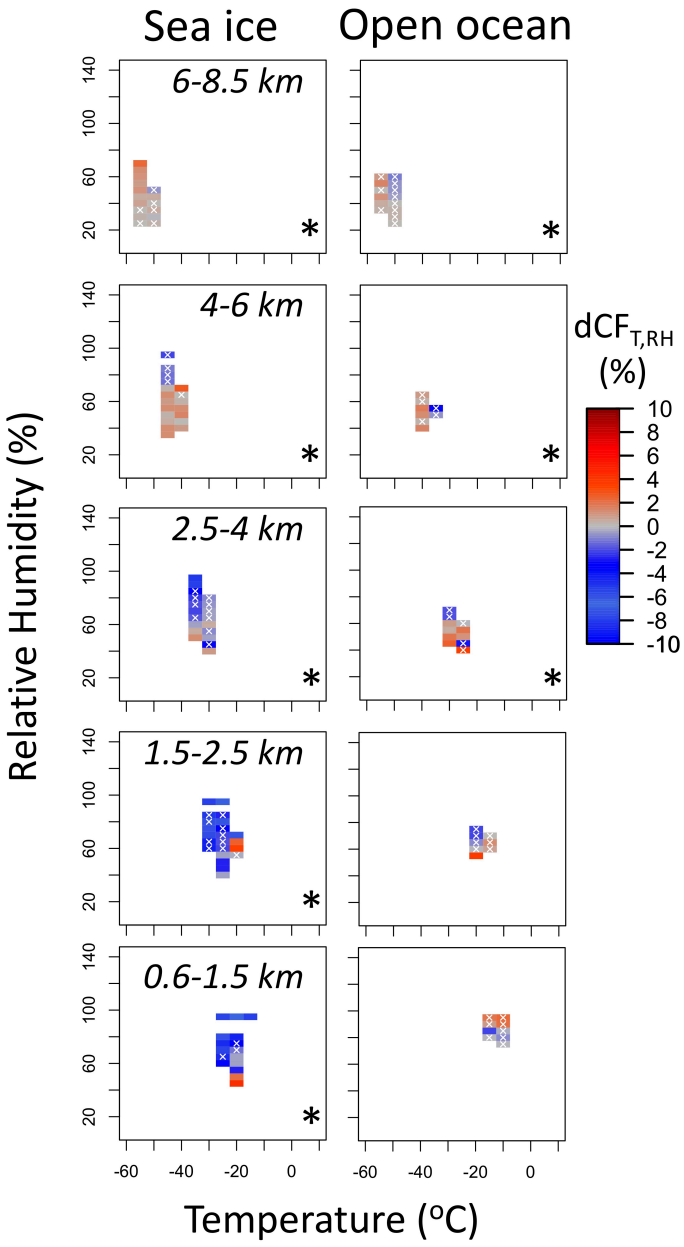

Figure S3. Same as for Figure S1, except for plotted only for Spring (March-May), and that the open ocean cases plotted above were only required to represent ≥ 5000 km^2 of gridded observations, as opposed to ≥ 7500 km^2. This plotted sample number distinction is purely for illustrative purposes, as the spring open ocean samples contained fewer clean cases for comparison than during the other seasons.

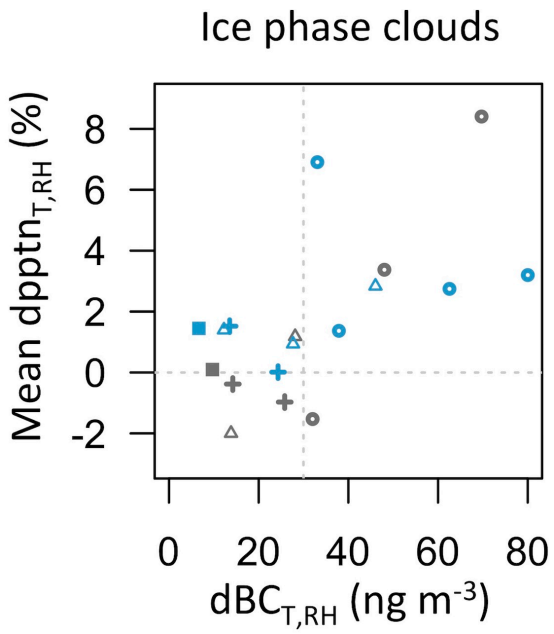

Figure S4. Mean IPC dpptn$_{T,RH}$ as a function of median dBC$_{T,RH}$ values within 10 ng m^{-3} BC increments. Values are shown for data over sea ice (grey) and open ocean (blue) at different altitudes between 0.6 and 6 km (open circles = 0.6-1.5 km, open triangles =1.5-2.5 km, crosses = 2.5-4 km, and filled squares = 4-6 km). In order to reduce the effects of outliers, each plotted data point represents at least 10 separate T/RH bins present in that altitude range, which in turn contain observations from at least 1250 km^2 over the Arctic Ocean. Thin light grey dashed lines indicate zero dpptn$_{T,RH}$ and a dBC$_{T,RH}$ value of 30 ng m^{-3}.

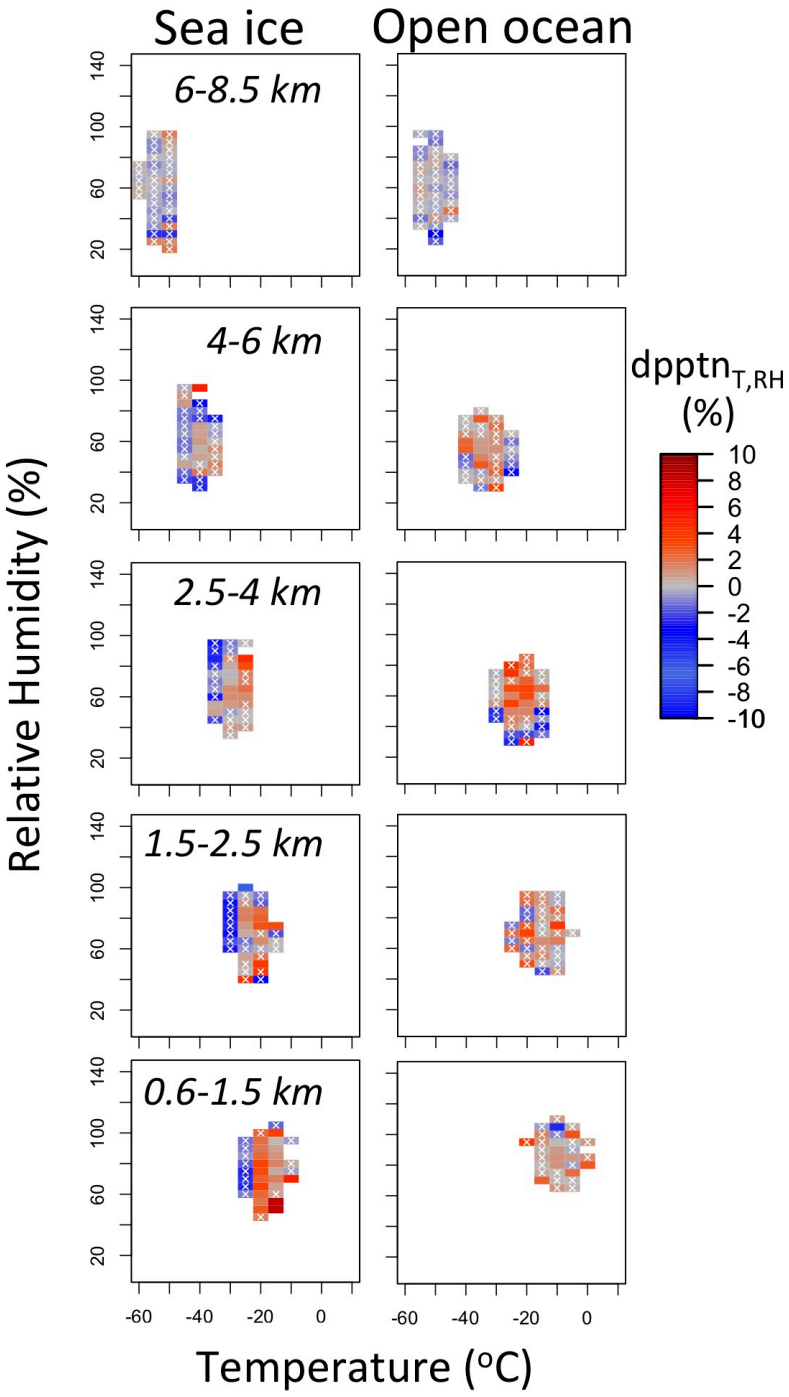

Figure S5. Same as for Figure 1, except for precipitation instead of cloud fraction. Here, individually significant cells numbered more than expected at random (binomial test, $p < 0.001$) at all levels except over open ocean between 1.5-2.5 km (significant at $p < 0.05$), and at 6-8.5 km (not significant).

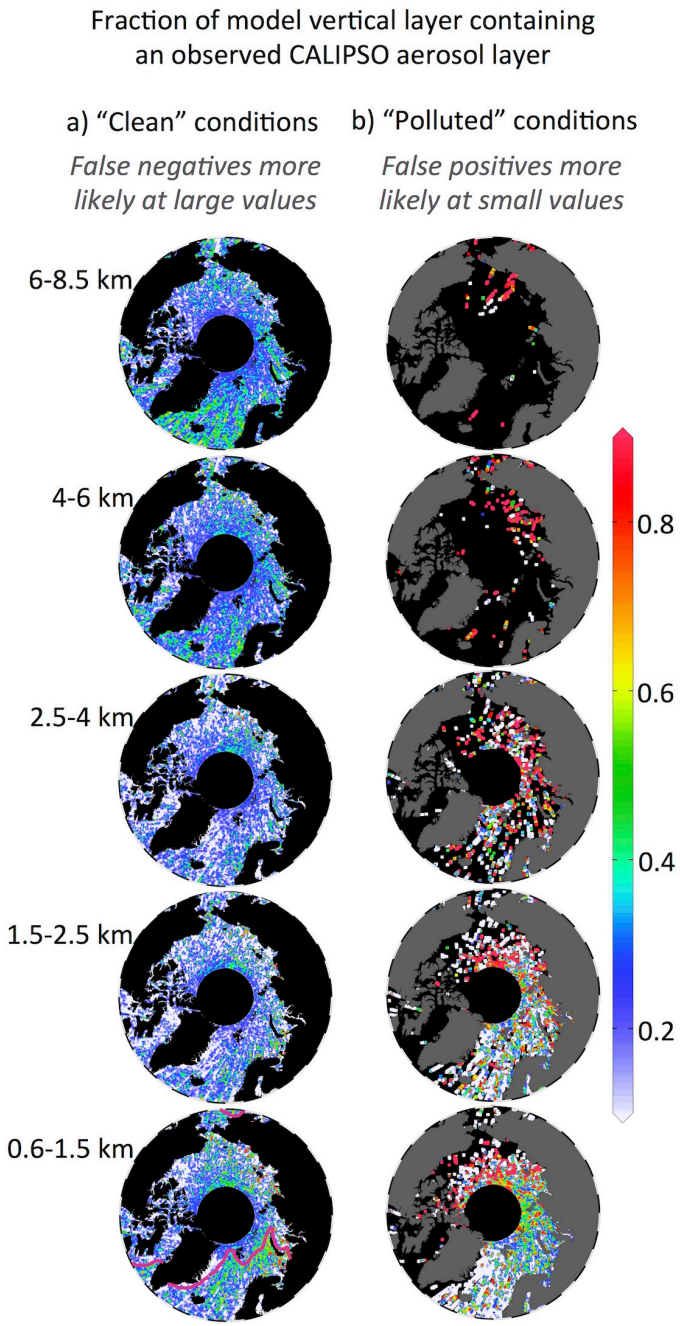

Figure S6. The fraction of different altitude layers in which CALIPSO aerosols were observed for the subsets of data with FLEXPART modeled BC concentrations a) < 30 ng m^{-3} (clean conditions), and b) > 150 ng m^{-3} (polluted conditions). Data are presented on a weighted average grid. Model false negatives are most likely to occur where fractions of the model vertical layer containing CALIPSO aerosols in (a) are high (i.e., closer to red in the color axis), because that indicates that the model predicted clean conditions, but CALIPSO aerosol layers were still frequently observed in that location. Model false positives are most likely to occur where these values in (b) are small (i.e., closer to white), because the model predicted a strong BC aerosol presence, but aerosol layers were not frequently observed by CALIPSO at that location. This interpretation is based

on the assumptions that combustion aerosols are associated with BC and that they are the dominant aerosol source at these altitudes during polar night. CALIPSO data were obtained in clear-sky nighttime conditions. The dark pink line on the bottom left represents sea ice extent during winter 2008-2009.

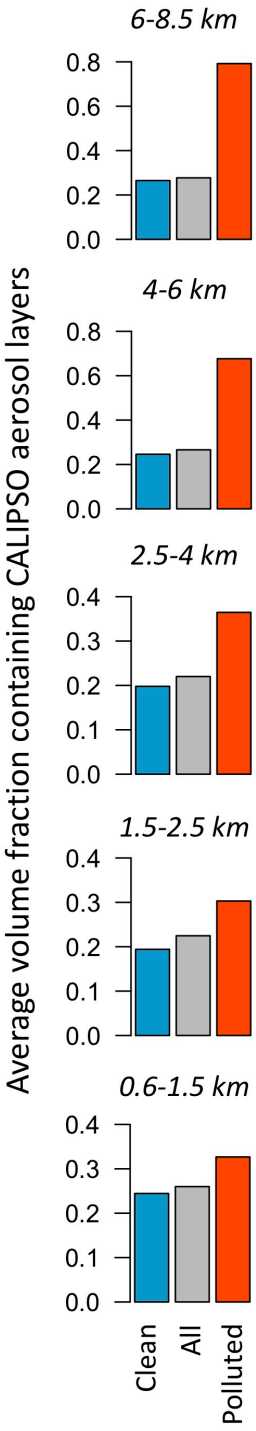

Figure S7. The average fraction of each altitude range containing observed CALIPSO aerosol layers for FLEPXART-determined clean (BC < 30 ng m^{-3}, blue), all (grey), and polluted (BC > 150 ng m^{-3}, red) conditions from ~500,000 clear air nighttime profiles between 2008-2009. Clean conditions had significantly smaller volumes occupied by aerosol layers than all or polluted conditions at every altitude, based on a Wilcoxon rank test, $p < 0.05$. Note different x-axes ranges in the plots.

Supplementary Tables

Table S1. The data shown in Figures 3 and 5, indicating $dCF_{T,RH}$ (%), $dpptn_{T,RH}$ (%), $dCP_{T,RH}$ (%) and $dBC_{T,RH}$ (ng m^{-3}) values in different altitude ranges over sea ice and open ocean, weighted by number of cloud observations in each T/RH bin ($\overline{dCF_{T,RH}}$, $\overline{dpptn_{T,RH}}$, $\overline{dCP_{T,RH}}$, and $\overline{dBC_{T,RH}}$, respectively). Data are presented at different altitude ranges, and separately for IPCs, MPCs, and LPCs. Values of $\overline{dCF_{T,RH}}$ and $\overline{dpptn_{T,RH}}$ are expressed as the absolute change within the air volume of interest, with the bootstrapped 95% confidence intervals for the weighted mean in round brackets. The values in square brackets are the relative percent change with respect to the value found in clean conditions. An asterisk (*) indicates significant differences between all and clean conditions based on a paired Wilcoxon rank test, $p < 0.05$, using T and RH grid cells containing > 800 (400) 12.5-km^2 gridded observations for $\overline{dBC_{T,RH}}$, $\overline{dCF_{T,RH}}$, and $\overline{dpptn_{T,RH}}$ ($\overline{dCP_{T,RH}}$). Values in bold indicate a significant change in $dCF_{T,RH}$, $dpptn_{T,RH}$ or $dCP_{T,RH}$ where $dBC_{T,RH}$ > 20 ng m^{-3} (Wilcoxon rank test, $p < 0.05$). The "Total (%)" values are the CP distributions in all conditions.

Altitude range (km)			*0.6-1.5*	*1.5-2.5*	*2.5-4*	*4-6*	*6-8.5*
Sea ice	Full dataset	$dBC_{T,RH}$ (ng m^{-3})	**27**	**21**	**14**	**7**	**3**
		$dCF_{T,RH}$ (%)	**-1.7 (-1.8 to -1.4) [-5.9]***	**-1.1 (-1.2 to -0.7) [3.5]***	**0.2 (0.1-0.5) [0.7]**	**0.7 (0.6-0.9) [3.5]***	0.4 (0.4-0.6) [3.5]*
		$dpptn_{T,RH}$ (%)	**0.9 (0.8-1.4) [3.0]***	**0.0 (-0.1-0.5) [0.1]**	**0.1 (-0.1-0.6) [0.3]**	-0.3 (-0.4-0.1) [-1.2]	-0.3 (-0.4-0.1) [-2.2]*
	Ice clouds	Total (%)	49	61	76	92	99
		$dCP_{T,RH}$ (%)	6.5 (6.3-7.3)*	**4.7 (4.4-5.4)***	1.7 (1.5-1.1)*	--	--
		$dpptn_{T,RH}$ (%)	-0.6 (-0.8 to 0.2)	0.3 (0.1-0.9)	0.5 (0.3-0.9)	0.2 (0.1-0.5)	-0.4 (-0.5 to -0.2)*
	Mixed phase clouds	Total (%)	35	36	23	8	1
		$dCP_{T,RH}$ (%)	-2.9 (-3.1 to -2.2)*	**-4.2 (-4.5 to -3.5)***	-1.7 (-1.9 to -1.1)*	--	--
		$dpptn_{T,RH}$ (%)	1.5 (1.3-2.1)*	1.3 (1.1-2.0)*	1.0 (0.8-1.7)	-0.1 (-0.3-0.4)	0.3 (-0.1-1.4)
	Liquid clouds	Total (%)	16	3	1	0	0
		$dCP_{T,RH}$ (%)	-3.7 (-3.8 to -3.1)*	**-0.4 (-0.5 to -0.1)***	0.0 (0.0-0.2)	--	--
		$dpptn_{T,RH}$ (%)	0.0 (0.0-0.0)	--	--	--	--
Open ocean	Full dataset	$dBC_{T,RH}$ (ng m^{-3})	**20**	**15**	**9**	**4**	**2**
		$dCF_{T,RH}$ (%)	-0.2 (-0.3-0.1) [-0.6]*	**1.4 (1.3-1.7) [3.8]***	1.1 (1.0-1.5) [4.2]*	0.5 (0.5-0.8) [2.3]*	0.8 (0.7-1.1) [4.0]*
		$dpptn_{T,RH}$ (%)	0.9 (0.8-1.3) [2.8]*	0.9 (0.7-1.3) [2.2]*	**0.4 (0.2-1.1) [1.2]***	0.7 (0.6-1.3) [3.1]*	-0.1 (-0.2 to 0.3) [-0.7]
	Ice clouds	Total (%)	30	39	58	78	93
		$dCP_{T,RH}$ (%)	0.6 (0.4-1.1)	**-0.6 (-0.8-0.1)**	-1.0 (-1.2 to -0.3)*	--	--
		$dpptn_{T,RH}$ (%)	0.6 (0.4-1.2)	1.1 (0.9-1.6)*	1.5 (1.3-2.1)*	0.9 (0.8-1.2)	-0.1 (-0.1-0.1)
	Mixed phase clouds	Total (%)	39	47	37	20	7
		$dCP_{T,RH}$ (%)	**0.5 (0.4-1.1)***	**0.7 (0.5-1.4)**	1.3 (1.1-2.0)*	--	--
		$dpptn_{T,RH}$ (%)	1.0 (0.7-1.6)*	0.1 (-0.1-0.7)	0.9 (0.7-1.6)	0.3 (0.1-0.9)*	-0.8 (-1.1 to -0.2)*
	Liquid clouds	Total (%)	31	15	6	1	0
		$dCP_{T,RH}$ (%)	-1.1 (-1.3 to -0.5)*	-0.2 (-0.3-0.3)	-0.3 (-0.3 to 0.0)	--	--
		$dpptn_{T,RH}$ (%)	0.1 (0.1-0.2)	-0.1 (-0.3-0.2)	-1.5 (-1.8 to -0.8)*	--	--